Slow-driving-induced multistability and remote synchronization in chaotic Chua's circuit

Tuhin Mahanty, Ayushi Saxena, and Sangeeta Rani Ujjwal
Department of Physics, Institute of Science, Banaras Hindu University, Varanasi, Uttar Pradesh 221005, India

(Received 8 January 2025; accepted 30 July 2026; published 24 August 2026)

We study the response of Chua's circuit driven by a chaotic signal of variable timescale. We observe that when the frequency of the driving signal is significantly lower than that of the response and the driving strength is above a threshold, Chua's circuit exhibits multiple stable attractors. The features of the attractors change as the driving strength ε increases; for instance, the attractors are double-scroll at low ε and are single-scroll when ε is high. We also investigate generalized synchronization (GS) between the drive and the response systems by employing the auxiliary system approach. When the drive is much slower than the response, we observe different scenarios of remote synchronization (RS) between response and auxiliary units. In addition to complete synchrony between response and auxiliary systems indicating GS between drive and response, we notice that the response and auxiliary units can be lag-synchronized and can also have correlated trajectories indicating novel forms of RS. The slow drive can induce multistability between these RS states, which disappears as the frequency of the driving signal increases and becomes equivalent to that of the response of Chua's circuit.

DOI: 10.1103/kwbg-sfbn

I. INTRODUCTION

The study of chaotic synchronization [1–3] has drawn considerable attention due to its potential applications in various areas such as chaos control [4,5] and secure communication [6,7]. Chaotic synchronization has been reported in several settings, from mutually coupled systems [8] to systems in drive-response configuration [9,10], and a wide variety of dynamical patterns such as global synchrony, lag synchronization, and generalized synchronization (GS) have been observed. Although a lot of investigation has been done to understand the dynamics of drive-response systems, most of these studies are limited to the case when drive and response have comparable timescales. Some experimental studies examined the synchronization of drive and response with timescale mismatch [11,12]. However, several aspects of the emergent phenomena in a system subjected to a driving signal with variable frequency are still unexplored. Through this work, we try to explore this direction further.

When nonidentical systems are coupled in the drive-response arrangement, they can synchronize in the generalized sense, namely, the state variable(s) of the response system can be expressed as a function of the state variable(s) of the drive [13]. One method to analyze this generalized synchronization (GS) between drive and response is to use the auxiliary system approach [14], wherein an exact copy of the response system (called the auxiliary system), driven by the same drive, is considered, and if the response and the auxiliary units are completely synchronized, then the response is said to be in generalized synchrony with the drive. This collective system of drive, response, and auxiliary units can be viewed as a three-node network in which the driving unit is acting like a hub and is unidirectionally coupled to the two unconnected nodes (drive and auxiliary systems). An important feature observed in such networks with hubs is the phenomenon of remote synchronization (RS), where the nodes that are not directly connected get synchronized, whereas these nodes remain out of synchrony with the hub [15]. Experimentally, electronic circuits are widely used to study chaotic synchronization, and, among these circuits, Chua's circuit [16,17] has emerged as a popular choice since it is one of the simplest electronic circuits to exhibit chaotic dynamics [18]. Chua's circuit and its variants [19] with different coupling schemes, for instance with resistive [20] and capacitive coupling [21], have been examined earlier [22,23].

In the present work, we study the dynamical properties of chaotic Chua's circuit driven by a chaotic signal of variable timescale. We observe that when the timescale of the drive is much slower than the response, and the driving strength is above a threshold, Chua's circuit exhibits bistability with the existence of two stable single-scroll attractors, although the dynamics of the uncoupled Chua's oscillator are on a double-scroll chaotic attractor. We also investigate the possibility of GS between the chaotic drive and Chua's circuit using the auxiliary system approach and found that when the driving strength is above a certain value, the response and the auxiliary units are in complete synchrony, implying GS between the drive and response systems. We note that the mismatch between the timescales of drive and response can induce novel types of RS wherein the response and auxiliary units are not coupled directly and oscillate with the same average frequency; however, their dynamical variables are related to each other in different ways: the response and auxiliary units can be in complete synchrony, lag synchrony, or can have correlated trajectories. The slow-varying drive can also induce multistability between these RS states. We analyze the effect of varying the timescale of the drive on the dynamics of Chua's circuit and on the GS between drive and response, both using circuit simulations on the platform MULTISIM and by numerically solving the dynamical equations. The response of Chua's circuit is studied by computing Lyapunov exponents of the system, and it is observed that, for a slow drive, the largest

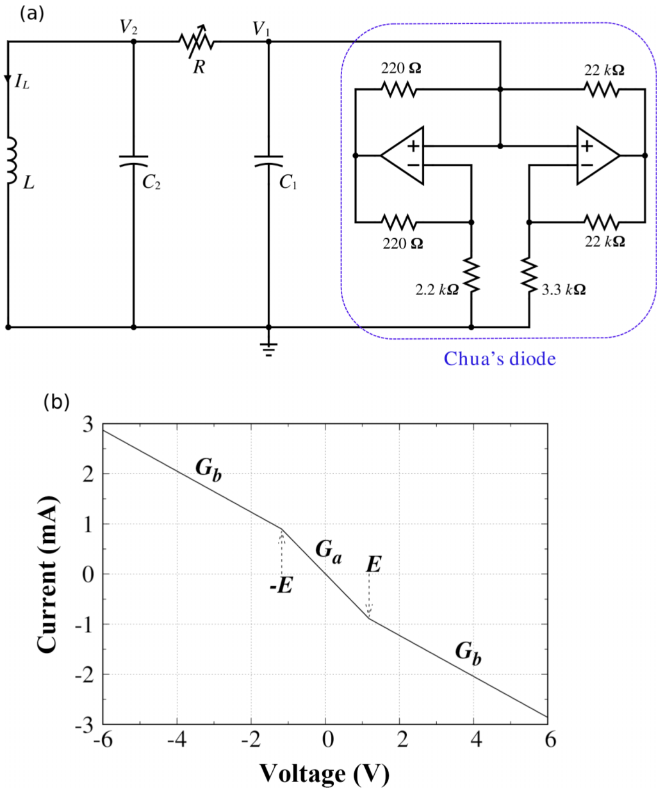

FIG. 1. (a) Circuit diagram of Chua's oscillator and (b) *V-I* characteristics of Chua's diode.

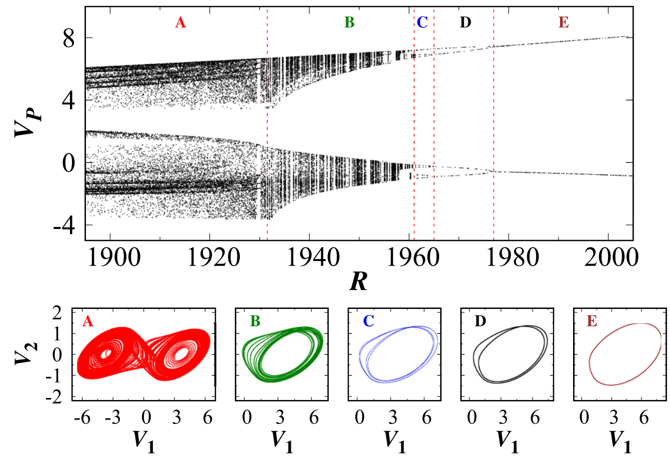

FIG. 2. Upper panel shows the bifurcation diagram of Chua's oscillator obtained by plotting the maxima V_P in the time series of V_1 as R varies, showing the period-doubling route to chaos and regions of existence of different types of attractors: double-scroll chaotic (A), single-scroll chaotic (B), period-4 (C), period-2 (D), and period-1 (E). The lower panel shows the attractors in different regions of the bifurcation diagram; for instance, at $R = 1920\ \Omega$ (A), 1950 Ω (B), 1963.5 Ω (C), 1970 Ω (D), and 2000 Ω (E) for a fixed initial condition [28]. Please note that we have presented only one variant of the single-scroll attractors in the bistable region (B to E).

conditional Lyapunov exponent (CLE) is close to zero in a significant coupling range. The dynamics of the response system in this region is investigated using measures such as the 0–1 test, a Fourier transform, and recurrence plots, which indicate the transition of the dynamics from periodic to chaotic through intermittency as the timescale of the drive varies. The drive is taken from a common base Colpitts oscillator [24]; however, we get qualitatively similar results for other chaotic drives as well.

The paper is arranged as follows: Section II describes the model considered for circuit simulation and numerical investigation. Multistability induced by driving is discussed in Sec. III. In Sec. IV, we analyze the generalized synchrony between drive and response by using the auxiliary system approach and present different scenarios of RS between response and auxiliary units. The investigation of the region of zero largest CLE using various tools is presented in Sec. V. The results are summarized in Sec. VI.

II. MODEL DESCRIPTION

We consider Chua's circuit [16,25] as the response system. The circuit representation of Chua's oscillator is shown in Fig. 1(a). The circuit parameters are taken to be $C_1 = 10$ nF, $C_2 = 100$ nF, $L = 18$ mH, and R is the variable resistor that controls the dynamics of Chua's oscillator. By applying Kirchhoff's circuit laws to various branches of this circuit, we get the following set of dynamical equations:

$$\begin{aligned}\dot{V}_1 &= \frac{1}{RC_1}[V_2 - V_1 - Rf(V_1)],\\ \dot{V}_2 &= \frac{1}{RC_2}(V_1 - V_2 + RI_L),\\ \dot{I}_L &= -\frac{V_2}{L},\end{aligned}\tag{1}$$

where the over-dot represents a derivative with respect to time. The characteristic equation of Chua's diode is given by

$$f(V_1) = G_bV_1 + \tfrac{1}{2}(G_a - G_b)(|V_1 + E| - |V_1 - E|),\tag{2}$$

where E is the turning point voltage and G_a, G_b are the slopes obtained from the *V-I* characteristics of Chua's diode plotted in Fig. 1(b). From the *V-I* characteristics of Chua's diode, we note that $G_a = -0.7574$ mA/V, $G_b = -0.4089$ mA/V, and $|E| = 1.18$ V. We use the software MULTISIM to simulate the circuit in the laboratory environment. The asymptotic dynamics of the system are verified using numerical simulation of the governing dynamical equations [Eq. (1)] using the Runge-Kutta fourth-order method, and the equivalence between the circuit and numerical simulations is established.

An interesting feature of Chua's circuit equations [Eqs. (1)] is that they remain invariant under parity transformation $[(V_1, V_2, I_L) \rightarrow (-V_1, -V_2, -I_L)]$ which can give rise to bistability of single-scroll attractors. In Chua's circuit, as the resistance R varies keeping other circuit elements constant, the dynamics of Chua's circuit change from periodic for larger R to chaotic for smaller R values [26,27]. The bifurcation diagram depicting the transition from periodic to chaotic dynamics is plotted in Fig. 2, which shows a period-doubling route leading to chaotic dynamics as R decreases. In Fig. 2,

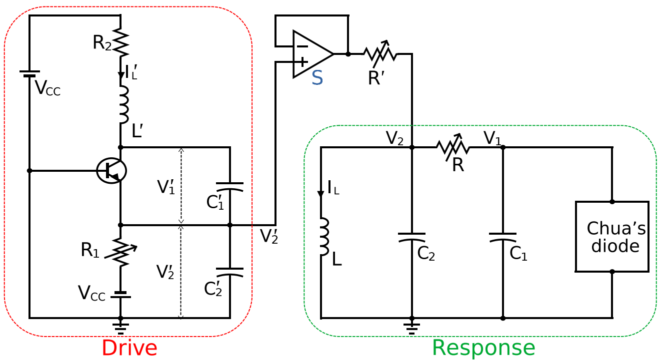

FIG. 3. Circuit diagram of Chua's circuit driven by a common base Colpitts oscillator.

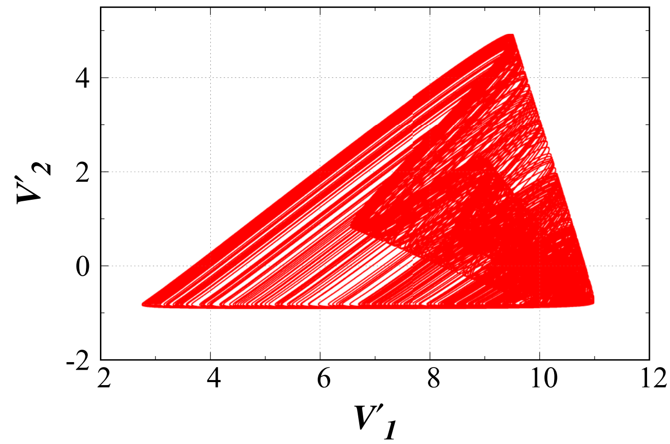

FIG. 4. The attractor of the Colpitts oscillator in the V_1'-V_2' plane.

the maxima of the time series of V_1 (denoted by V_P) are plotted, taking random initial conditions [29] at each R. We note that, depending on the initial conditions, two variants of the single-scroll attractors are possible: one with positive V_1 values and the other with negative V_1 values in phase space. In the lower panel of Fig. 2, the attractors (V_1 vs V_2) obtained for different values of R are shown. We have shown only one variant of the single-scroll attractor (having positive V_1 values) in the bistable region. As can be seen, periodic attractors are obtained for high values of R: period-1 for $R = 2000\ \Omega$, period-2 for $R = 1970\ \Omega$, and period-4 for $R = 1963.5\ \Omega$. For lower values of R, for instance, when $R = 1950\ \Omega$ and when $R = 1920\ \Omega$, single-scroll and double-scroll chaotic attractors are obtained, respectively.

III. MULTISTABILITY IN THE DRIVEN CHUA CIRCUIT

Chua's circuit is driven by a chaotic signal taken from a common base Colpitts oscillator [24,30]. The circuit diagram of the Chua's circuit driven by a Colpitts oscillator is shown in Fig. 3. From the circuit, the dynamical equations of the Colpitts oscillator can be written as

$$\dot{V}_1' = \frac{\Phi}{C_1'}[I_L' - \alpha I_s(e^{-\frac{V_2'}{V_T}} - 1)],$$
$$\dot{V}_2' = \frac{\Phi}{C_2'}\left[I_L' + I_s(1-\alpha)(e^{-\frac{V_2'}{V_T}} - 1) - \frac{V_{CC} + V_2'}{R_1}\right],$$
$$\dot{I}_L' = \frac{\Phi}{L'}(V_{CC} - V_1' - V_2' - I_L' R_2). \tag{3}$$

Here $C_1' = C_2' = 0.5\ \mu\text{F}$, $L' = 20\ \text{mH}$, $R_1 = 5000\ \Omega$, $R_2 = 100\ \Omega$, and $V_{CC} = 10\ V$. $I_s = 10^{-16}$ A is the reverse saturation current of the transistor, $\alpha = 0.995$ is the gain of the transistor, and $V_T = 0.0258$ V is the temperature coefficient [24]. The attractor of the Colpitts oscillator in the V_1'-V_2' plane is shown in Fig. 4. In Eqs. (3), we introduce a parameter Φ to control the timescale of the driving signal. In circuit realization, this is done by modifying the values of capacitors and inductor as $C_1' \to \frac{C_1'}{\Phi}$, $C_2' \to \frac{C_2'}{\Phi}$, and $L' \to \frac{L'}{\Phi}$.

We fix the circuit parameters to the values mentioned earlier, and the resistance R is fixed to $R = 1920\ \Omega$ so that the undriven Chua's circuit is in a chaotic regime with asymptotic dynamics on the double-scroll attractor [31]. To study the effect of the external chaotic drive on Chua's circuit, we fed the voltage V_2' from the Colpitts oscillator through a unidirectional switch S and a resistance R' at V_2 of Chua's circuit.

The dynamical equations for the driven Chua's circuit read

$$\dot{V}_1 = \frac{1}{RC_1}[V_2 - V_1 - Rf(V_1)],$$
$$\dot{V}_2 = \frac{1}{RC_2}(V_1 - V_2 + RI_L) + \varepsilon(V_2' - V_2),$$
$$\dot{I}_L = -\frac{V_2}{L}. \tag{4}$$

Here V_2' is used as the driving signal and ε denotes the driving strength expressed as $\varepsilon = \frac{1}{R'C_2}$. In the circuit, the coupling strength ε is varied by changing R' while keeping C_2 constant. Here we are interested in studying the response of Chua's circuit for different timescales of the drive. The time series of V_2' of the Colpitts oscillator for different values of the timescale parameter Φ are plotted in Fig. 5 to compare them with the timescale of Chua's oscillator.

The average time period, $\bar{T}$ of the driving signal is calculated by noting the time duration, Δt between consecutive peaks in the time series and taking the average over many such peaks. The inverse of $\bar{T}$ gives the average frequency $\bar{\nu}$ such that

$$\bar{T} = \frac{\sum_{i=1}^{N} \Delta t_i}{N},$$

and

$$\bar{\nu} = \frac{1}{\bar{T}},$$

where N is the total number of peaks in the chosen time interval of the time series.

The average frequency $\bar{\nu}$ of the V_1 variable of Chua's oscillator in the chaotic regime ($R = 1920\ \Omega$) and the chaotic driving signal V_2' for several values of the timescale parameter Φ are shown in Table I. We note that the average frequency of the driving signal $\bar{\nu}$ varies linearly with the timescale parameter Φ.

The bifurcation diagram for the driven Chua's circuit with increasing ε gives an overview of the possible attractors. In Fig. 6 we plotted the maxima of V_1 (denoted by V_p) for a random initial condition for each ε. Here we observe that when

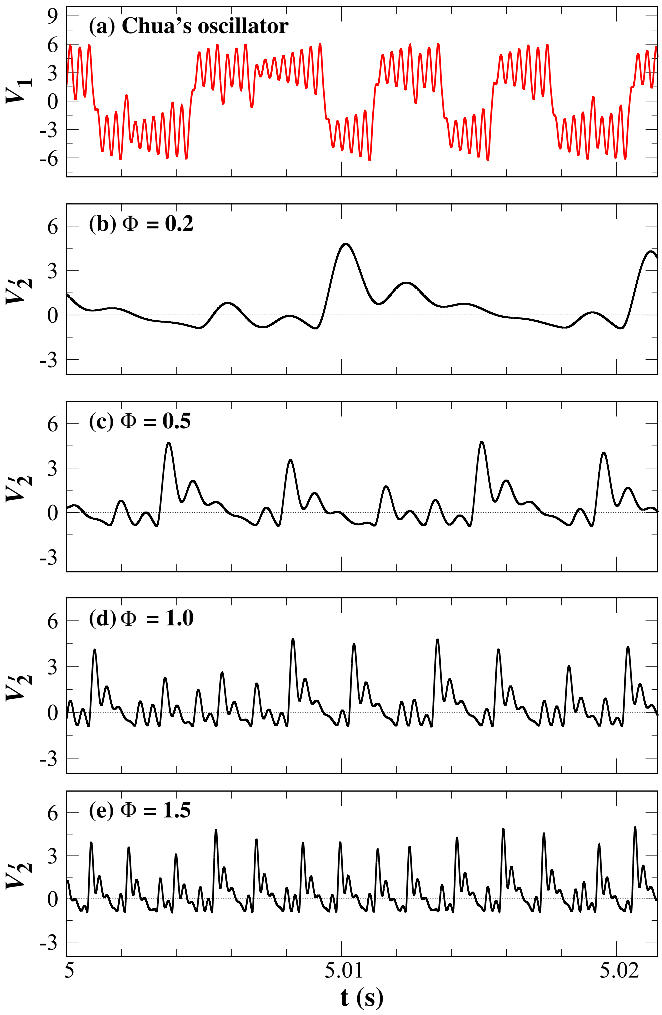

FIG. 5. Time-series of (a) V_1 of the response of Chua's circuit at $R = 1920\ \Omega$, and (b)–(e) driving signal (V_2') at different values of timescale parameter Φ obtained from circuit simulation.

the driving signal is much slower than the response, indicated by a small value of Φ [Fig. 6(a)], the asymptotic dynamics of Chua's circuit is on a double-scroll chaotic attractor when the driving strength ε is low. As ε increases (for fixed Φ), the attractor changes from double-scroll to single-scroll. As we can see in Fig. 6(a), there are two variants of single-scroll chaotic attractors corresponding to the upper (b_+) and lower (b_-) branches in the bifurcation diagram. For the branch b_+,

TABLE I. Comparison of average frequency of Chua's oscillator and the frequency of chaotic drive for different values of timescale parameter Φ.

Φ	Average time period $\bar{T}$ (s)	Average frequency $\bar{\nu}$ (Hz)
0.2	2.427×10^{-3}	412
0.5	9.8×10^{-4}	1021
1.0	4.923×10^{-4}	2031
1.5	3.238×10^{-4}	3088
Chua's Circuit	3.370×10^{-4}	2967

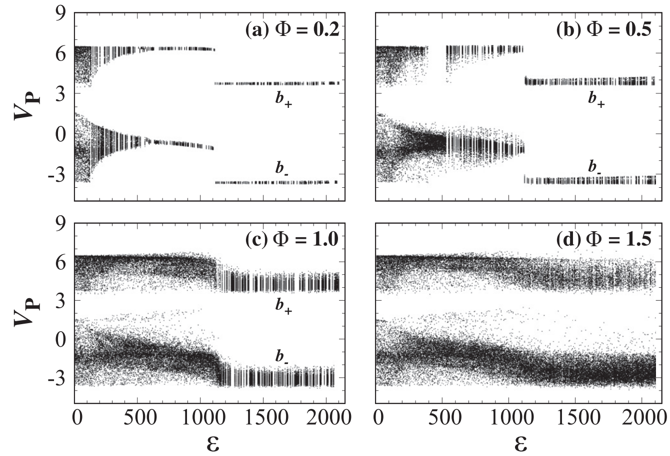

FIG. 6. Bifurcation diagram of the driven Chua's circuit with increasing coupling strength ε for different values of the timescale parameter Φ, taking random initial conditions at each ε.

the attractor has positive V_1 values and is denoted by A_+, whereas for b_- the attractor has negative V_1 values and is referred to as A_-. We also observe that the size of these single-scroll chaotic attractors (A_+ and A_-) decreases with an increase in driving strength ε, as evident from the attractors plotted in Fig. 7. On the contrary, when the timescale of drive is comparable to that of response, the long-time dynamics of the response always remains on the double-scroll chaotic attractor [Fig. 6(d)]. The shape of the attractors of the driven Chua's oscillator for different values of Φ and ε is shown in Fig. 7, showing bistability in the parameter region where the single-scroll attractors exist.

We also study the transition of the attractor from double-scroll to single-scroll in the parameter space of Φ and ε. To distinguish between single-scroll and double-scroll attractors, we consider the time series of V_1 after removing the transients

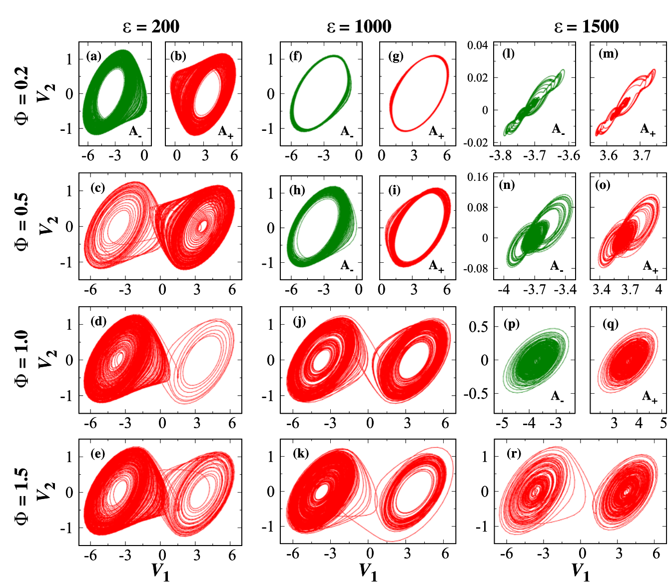

FIG. 7. Attractors of driven Chua's circuit are plotted for different values of the timescale parameter Φ and driving strength, ε.

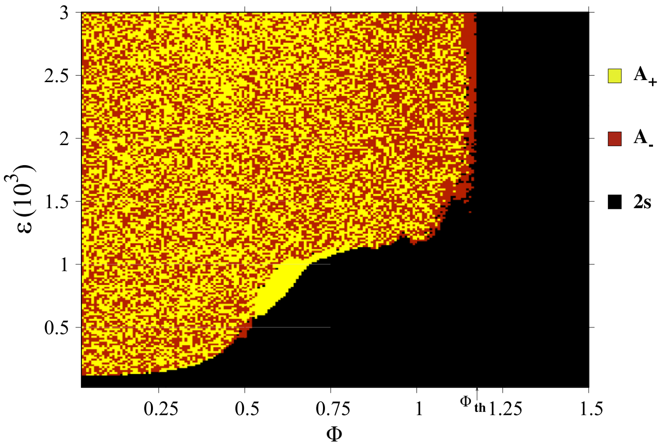

FIG. 8. Figure showing existence of double-scroll (2s) and single-scroll (A_+ and A_-) attractors for the driven Chua's circuit in Φ-ε parameter space with initial conditions taken randomly [29].

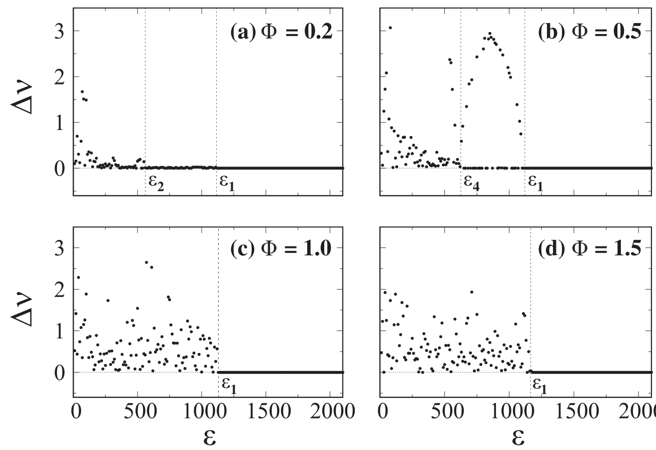

FIG. 9. Plot of the difference in average frequency between the response and auxiliary Chua oscillators, $\Delta\nu$ as a function of driving strength, ε for different values of Φ taking random initial conditions at each ε.

and take the maxima, $V_{1(\max)}$, and minima, $V_{1(\min)}$, of the time series. We compute the quantity χ defined as $\chi = V_{1(\max)} + V_{1(\min)}$. If $\chi \approx 0$, the dynamics of Chua's oscillator is on the double-scroll attractor, whereas χ positive (>5) and negative (<-5) indicate that the trajectories converge to A_+ and A_- attractors, respectively. As seen in Fig. 8, the transition from a double-scroll to a single-scroll attractor occurs at a lower value of ε, when the drive is much slower than the response (low value of Φ). As Φ increases, the point of transition moves toward higher ε. When the timescale of the drive approaches that of the response, there is no transition from double-scroll to single-scroll chaotic attractor, and we observe double-scroll attractors in the entire ε range. This threshold value of Φ beyond which only double-scroll attractors are observed is marked as Φ_{th} ($\approx$1.18) in Fig. 8. From these observations, we conclude that a slow driving signal favors the existence of single-scroll chaotic attractors and hence bistability in the driven Chua's circuit.

IV. GENERALIZED SYNCHRONIZATION IN DRIVEN CHUA'S CIRCUIT

Nonidentical unidirectionally coupled systems can achieve synchronization in a generalized manner wherein the dynamical variables of the response system can be expressed as a function of the dynamical variables of the drive [13]. One way to study the generalized synchrony between response and drive is to employ the auxiliary system approach [14] where an identical copy of the response system, known as the auxiliary system, is considered and the common driving signal is fed to both response and auxiliary units. If the response and auxiliary systems are completely synchronized, then the response is said to be in generalized synchrony with the drive.

To study the generalized synchrony between Chua's circuit and the chaotic drive, we consider an identical Chua system as an auxiliary with dynamical variables denoted by V_1^a, V_2^a, and I_L^a, where the superscript a is used to distinguish the state variables of the auxiliary system from those of the response Chua's circuit.

The asymptotic dynamics of the two Chua circuits (response and auxiliary) are on the double-scroll chaotic attractor (fixing $R = 1920\ \Omega$) when no driving signal is applied. To investigate the nature of generalized synchrony between drive and Chua oscillator, we force the response and auxiliary systems by a common chaotic signal V_2' of the common base Colpitts oscillator.

The synchronization between the response and auxiliary units is studied as a function of coupling strength, ε for a fixed value of the timescale parameter Φ. As ε increases (for fixed Φ), the trajectories of the two Chua oscillators transition from being desynchronized to a synchronized state at a coupling threshold marked as ε_1. To identify this threshold we plot the difference of average frequency, $\Delta\nu = |\bar{\nu} - \bar{\nu}^a|$ of the two Chua oscillators as a function of ε for different Φ in Fig. 9. When the timescale of drive is much slower than the response, the transition from desynchronized ($\Delta\nu \neq 0$) to the complete synchronized state ($\Delta\nu = 0$) is through a region of multistability where the synchronized state coexists with other states for which $\Delta\nu \approx 0$ (between ε_1 and ε_2), shown in Fig. 9(a). As Φ increases, the difference in average frequencies increases, and there is a region in ε space where the synchronized state exists with the desynchronized state, as indicated by scattered points for intermediate values of ε (region between ε_1 and ε_4) in Fig. 9(b). This multistability of synchronization and desynchronization between response and auxiliary units disappears as the timescale of the drive increases and becomes equivalent to the timescale of the response [Figs. 9(c) and 9(d)].

To probe further into the features of the emerging states as Φ and ε vary, we calculate the similarity parameter [32] between the time series of the state variables V_1 and V_1^a of the response and the auxiliary, respectively. The similarity parameter $S(\tau)$ is defined as

$$S(\tau) = \sqrt{\frac{\langle [V_1^a(t+\tau) - V_1(t)]^2 \rangle}{[\langle (V_1(t))^2 \rangle \langle (V_1^a(t))^2 \rangle]^{\frac{1}{2}}}}, \tag{5}$$

where τ is the time shift considered between the time series of the two driven Chua circuits and $\langle . \rangle$ denotes the time averages.

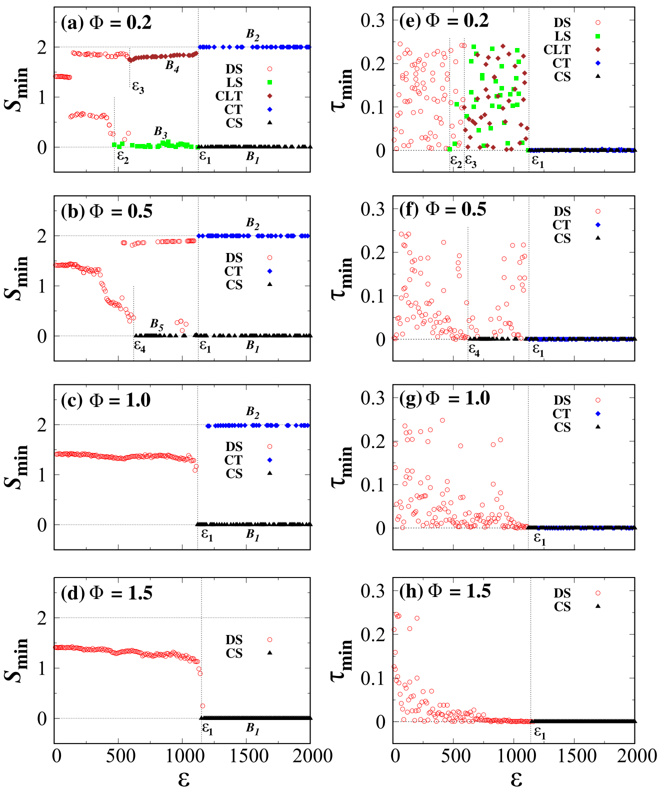

FIG. 10. The minimum of similarity parameter $S_{\min}$ (left panel) and the corresponding $\tau_{\min}$ (right panel) with increasing ε for different values of timescale parameter, Φ showing complete synchronization (CS with black triangles), correlated trajectories (CT with blue diamonds), lag synchronized state (LS with green squares), correlated lag trajectories (CLT with brown filled diamonds), and desynchronized state (DS with red circles).

The minimum value of the similarity parameter, $S_{\min}$, and the corresponding $\tau_{\min}$ are plotted in Fig. 10 as a function of driving strength ε for different values of the timescale parameter Φ. We observe that depending on the values of Φ, ε, and the initial conditions for the state variables, the two Chua oscillators can be in one of the following states:

(1) Complete synchronization (CS), where

$$\begin{aligned} V_1(t) &= V_1^a(t), \\ V_2(t) &= V_2^a(t), \\ I_L(t) &= I_L^a(t). \end{aligned} \tag{6}$$

(2) Lag synchronization (LS) where

$$\begin{aligned} V_1(t) &= V_1^a(t+\Delta t), \\ V_2(t) &= V_2^a(t+\Delta t), \\ I_L(t) &= I_L^a(t+\Delta t). \end{aligned} \tag{7}$$

Here Δt is the time lag between the time series of the state variables of response and auxiliary systems.

(3) Correlated trajectories (CT) where

$$\begin{aligned} V_1(t) &= V_1^a(t) + k_1, \\ V_2(t) &= V_2^a(t), \\ I_L(t) &= I_L^a(t) + k_2. \end{aligned} \tag{8}$$

k_1 and k_2 are time-independent constants. These constants are the same for all ϵ for a fixed Φ.

(4) Correlated lag trajectories (CLT) where

$$\begin{aligned} V_1(t) &= -V_1^a(t+\Delta t), \\ V_2(t) &= -V_2^a(t+\Delta t), \\ I_L(t) &= -I_L^a(t+\Delta t). \end{aligned} \tag{9}$$

Here Δt is the time lag. In the CLT state, the response and the auxiliary systems are in antiphase synchrony and follow Eq. (9) for most times.

(5) Desynchronized state (DS) where there is no correlation between the state variable of the response and auxiliary Chua oscillators.

For CS, $S_{\min} = 0$ at $\tau = 0$ whereas $S_{\min} \simeq 0$ for $\tau \neq 0$ represents LS. For DS, the similarity parameter $S_{\min} \gg 0$ for all τ values [32]. To differentiate and verify the existence of different states, we modify the similarity parameter as

$$S_{\mathrm{mod}}(\tau) = \sqrt{\frac{\langle [(V_1^a(t+\tau)+k) \pm V_1(t)]^2\rangle}{[\langle (V_1(t))^2\rangle \langle (V_1^a(t))^2\rangle]^{\frac{1}{2}}}}. \tag{10}$$

For the CS, LS, and CLT states, $k = 0$, while k is finite for the CT state. For the CLT states, we consider the $+$ sign to verify the relation between the state variables [Eq. (9)], whereas the $-$ sign applies for the other states. From Fig. 10 we observe that, when driving is much slower than the response ($\Phi = 0.2$), for low values of driving strength ε, the two Chua oscillators are in DS, indicating no GS between the Chua circuit and the drive. As ε increases and crosses a threshold value, we see two branches B_3 ($\varepsilon_2 < \varepsilon < \varepsilon_1$) and B_4 (after $\varepsilon_3 < \varepsilon < \varepsilon_1$) emerging from the desynchronized region. The branch B_4 corresponds to the CLT state where response and auxiliary go to two different attractors (A_+A_- or A_-A_+) and also have a time lag, while B_3 represents LS between the two Chua oscillators. These two branches indicate different scenarios of remote synchronization (RS) where two Chua circuits not directly coupled to each other synchronize (indicated by equal average frequency) via a common drive but have different phase relations between their dynamical variables. Therefore, one can anticipate some relationship between the dynamics of the response Chua oscillator and the drive. We call the RS between the two Chua oscillators corresponding to the two branches B_3 and B_4 as RS of type III (RS-III) and RS of type IV (RS-IV), respectively. As ε increases further, exceeding ε_1 the lag synchronized branch (B_3) evolves to complete synchrony (CS) denoted by B_1 while the CLT changes to CT state (B_2 branch) where the two Chua oscillators go to two different single-scroll attractors (A_+ or A_-) with no time lag but there is a correlation between the state variables of the two oscillators given in Eq. (8). The state CT seems to indicate a new kind of RS between the drive and the response systems, which we name remote synchronization of type II (RS-II). Therefore, in addition to the case when the response and auxiliary systems are in complete synchrony (CS), say RS-I, which indicates generalized synchrony between the drive and response, we observe new scenarios of remote synchronization, namely, RS-II, RS-III, and RS-IV, where the trajectories of response and auxiliary Chua oscillators are correlated in a different manner. Moreover, in Fig. 10(a) we observe two regions of multistability: one at intermediate values of ε (between ε_3 and ε_1) where RS-III coexists with RS-IV (LS coexists with CLT) and another at higher ε where RS-II coexists with RS-I (CS coexists with CT). The latter region appears more interesting because it shows the coexistence of remote synchronization with generalized synchronized states.

For higher values of the timescale parameter Φ, the lag between the time series of the Chua oscillators decreases, and the LS state converts into CS while the CLT branch becomes desynchronized [Fig. 10(b)]. This gives rise to a multistable region between ε_4 and ε_1 where CS and DS coexist, and one can expect chimera-like states [33,34] to emerge in an ensemble of Chua oscillators driven by a common chaotic signal. Therefore, as Φ increases, the LS and CLT states disappear, and the bistability is between CS and CT states only for $\varepsilon > \varepsilon_1$ [Fig. 10(c)]. Further increasing Φ makes the CT state vanish, and when the timescale of the drive is equivalent to that of the response ($\Phi \approx 1.46$), only CS exists above a critical coupling, ε_1. This investigation indicates that a significantly slower drive induces novel types of RS and multistability in the drive-response system, which disappear when the timescale of the drive is comparable to that of the response.

The attractors (left panels) and the time series (right panels) obtained from circuit simulation for these different states are shown in Fig. 11. To illustrate the agreement between results obtained from circuit simulations and numerical integration of model equations, the attractors obtained numerically are shown in Figs. 11(h)–11(n). We observe that, for low Φ the synchronization of response and auxiliary is on a single-scroll attractor, whereas for high Φ, the synchronization is on a double-scroll attractor. For the lower frequency of the drive, CS can be on two types of single-scroll attractors: one with positive V_1 and V_1^a values denoted by CS(up) and the other with negative V_1 and V_1^a values marked as CS(down) in Fig. 11. Also, the size of the single-scroll attractor on which dynamics is synchronized decreases with an increase in ε. For higher Φ, LS, and CLT are the first to disappear, and then CT disappears when complete synchronization of the two Chua oscillators occurs on the double-scroll attractor indicated by CS(2s).

To analyze the stability of the synchronized states, we compute the conditional Lyapunov exponent for the driven Chua circuit. In Fig. 12, the largest conditional Lyapunov exponent λ_m is plotted as a function of coupling strength ε for different values of Φ. We observe that, for low values of ε, λ_m is positive, suggesting incoherence between the two Chua oscillators and hence no GS between drive and response. After the driving strength crosses the threshold ε_1, λ_m becomes negative, indicating GS between the drive and the response systems [9]. The value of $\lambda_m \approx 0$ when there is lag synchronization (LS) between the trajectories of the response and auxiliary units. In the region where RS-III coexist with RS-IV, λ_m has either small positive or negative values depending on the initial conditions. From Figs. 12(c) and 12(d), we notice that, for higher values of Φ, the desynchronized region expands and we are unlikely to get LS and CLT states. We also note that λ_m is negative in the parameter region where RS-I and RS-II coexist. The Lyapunov exponent spectrum for the driven system is also plotted (see Fig. 13). The drive-response system will have six Lyapunov exponents (LEs). We observe that, for low coupling ε, the drive-response system is hyperchaotic, characterized by two positive LEs. One LE is always positive due to the chaotic nature of the drive. At ε_1 and ε_2, one or more LEs come close to zero (avoided crossing), indicating a change in the system's dynamics (response in this case, since the drive remains unaffected by the coupling). If we separate the LEs corresponding to the drive, we will be left with three LEs that represent the dynamical nature of the response. Doing this, we found that the largest LE of the response system is close to zero in the range $\varepsilon_2 < \varepsilon < \varepsilon_1$ whereas it is negative when $\varepsilon > \varepsilon 1$.

To confirm the generalized synchronization (GS) between the response Chua's circuit and the drive, we plot V_1^a vs V_1 in Fig. 14. V_1^a varies linearly with V_1 for CS and CT, indicating GS between drive and response. When the synchronization is on the single-scroll attractor, the plots for CS lie either in the first or third quadrant while plots for CT lie in the second or fourth quadrants in V_1-V_1^a space. At higher Φ, when the synchronization is on a double-scroll attractor only, the plots are in the form of a straight line stretching through the first and third quadrants and passing through the origin. For DS, the variation of V_1^a with respect to V_1 is random, whereas the plots look like closed orbits for CLT and LS states, indicating some correlation between the trajectories of response and auxiliary units.

Since the driven Chua's circuit exhibits multistability, we examine the fraction of initial conditions leading to various attractors. For a fixed ε, we take 10^3 initial conditions randomly and compute the fraction of initial conditions, f_{ic} going to various states: CS(up), CS(down), CS(2s), and CT (see Fig. 15). The figure confirms that when Φ is below a certain value Φ_{th}, the synchronization between response and auxiliary is on the single-scroll attractors marked as CS(up) (when the synchronization is on A_+) and CS(down) (when the synchronization is on A_-) or there could be scenario where one oscillator asymptotes to A_+ and the other goes to A_- or vice versa, termed the "CT state". When $\Phi > \Phi_{\mathrm{th}}$, the two Chua oscillators synchronize onto the double-scroll attractors [CS(2s)]. Therefore, it can be concluded that when the drive has a lower frequency than the response, we expect synchronization on a single-scroll attractor and hence multistability of various kinds, while when the frequency of the drive is comparable to the response, the synchronized dynamics is on a double-scroll attractor only and hence no multistability.

V. ANALYSIS OF DYNAMICS IN THE $\lambda_m = 0$ REGION

To understand the dynamical nature of a driven Chua circuit in the region where $\lambda_m \approx 0$, we analyze the time series of the response system at different Φ and fixed coupling ϵ using various measures such as the 0–1 chaos test, a fast Fourier transform (FFT), and recurrence plots.

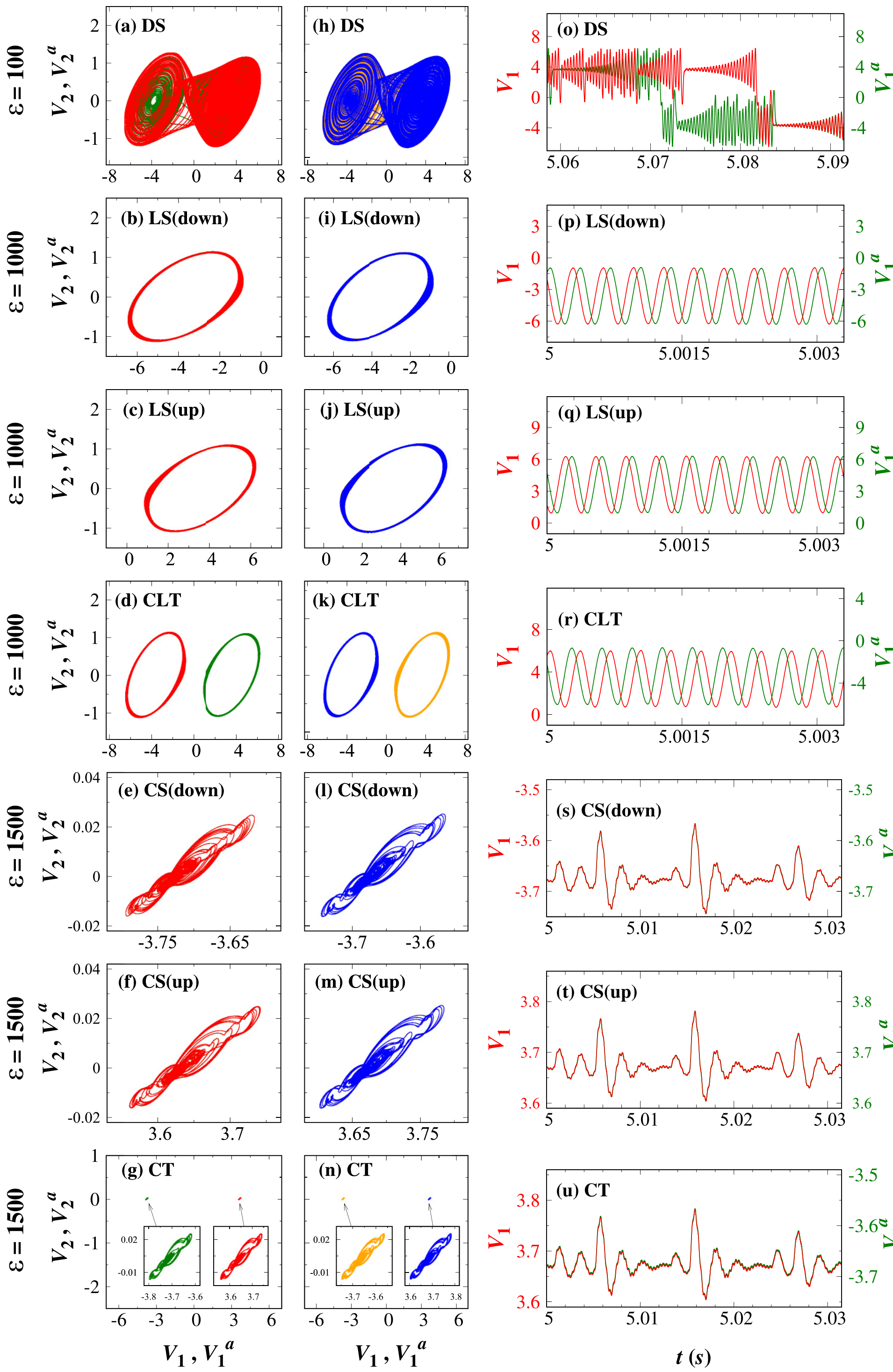

FIG. 11. Attractors of the response (in red) and auxiliary (in blue) Chua's circuits obtained from circuit simulation in MULTISIM [right panels (a)–(g)] and numerically [middle panels (h)–(n)] for various observed states DS, LS, CLT, CS, and CT for $\Phi = 0.2$. The right panel shows the time-series plots of V_1 of the response (red color) and V_1^a (blue color) of the auxiliary signal obtained numerically.

A. 0–1 chaos test

The 0–1 test is designed to distinguish chaotic behavior from regular dynamics in deterministic systems. If the outcome of the test is 1, it indicates the chaotic nature of the system, whereas a 0 result corresponds to regular dynamics. For the implementation of the 0–1 test, we follow the steps outlined in Ref. [35]. We consider the time series of V_1 of length N and define translation variables $p(n)$ and $q(n)$ as

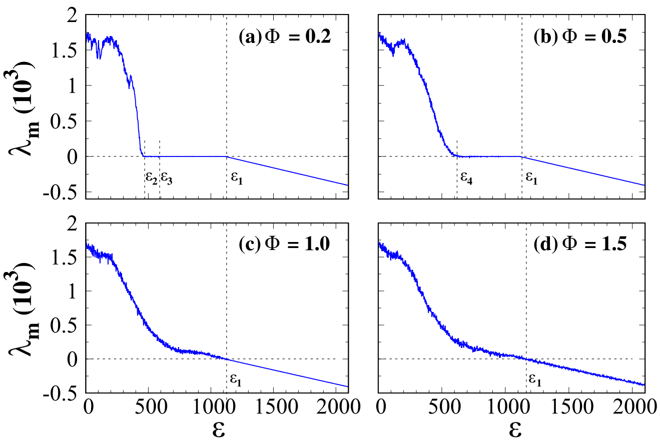

FIG. 12. The largest conditional Lyapunov exponent λ_m with varying ε for different timescales of the drive, Φ.

follows:

$$p(n) = \sum_{j=1}^{n} \eta(j)\cos(jc),$$

$$q(n) = \sum_{j=1}^{n} \eta(j)\sin(jc), \tag{11}$$

where $\eta = 1, 2, \ldots, N$ and $\eta(j)$ is a observable constructed from the time series.

The value of c can be chosen from the interval $(0,\pi)$. The behavior of these translational variables determines whether the dynamics is chaotic or regular. To determine the diffusive or nondiffusive behavior of p and q, we calculate the mean squared displacement $M(n)$ as

$$M(n) = \lim_{N\to\infty} \frac{1}{N} \sum_{j=1}^{N} [p(j+n) - p(j)]^2 + [q(j+n) - q(j)]^2. \tag{12}$$

For large N, we require $n \ll N$. Hence, we calculate $M(n)$ for $n \leqslant N_c$ such that $N_c \ll N$. We take $N_c = N/10$ for our analysis. For better convergence of $M(n)$, a modified mean squared displacement $D(n)$ is used, which is defined as

$$D(n) = M(n) - V_{\text{osc}}(c, n), \tag{13}$$

where

$$V_{\text{osc}}(c, n) = \lim_{N\to\infty} \frac{1}{N} \sum_{j=1}^{N} \eta(j)^2 \frac{1-\cos(nc)}{1-\cos(c)}. \tag{14}$$

We compute the asymptotic growth rate K for a particular value of c $(c = 2)$ from $D(n)$ by the correlation method, in which K is defined as the correlation coefficient of the vectors

$$\zeta = (1, 2, \ldots, N_c),$$

and

$$\Delta = (D(1), D(2), D(3), \ldots, D(N_c)), \tag{15}$$

such that

$$K = \text{corr}(\zeta, \Delta) = \frac{\text{cov}(\zeta, \Delta)}{\sqrt{\text{var}(\zeta)\text{var}(\Delta)}} \in [-1, 1], \tag{16}$$

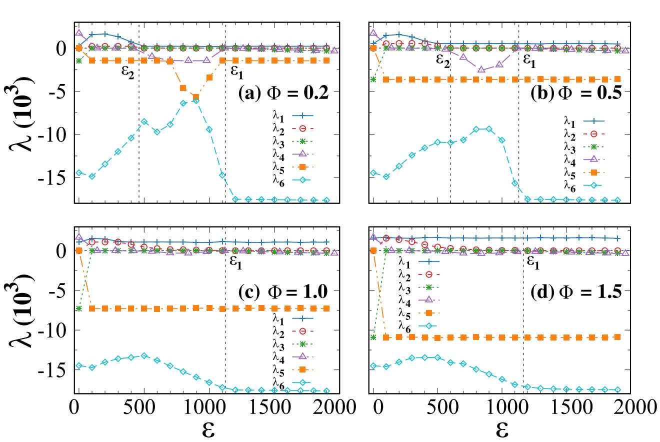

FIG. 13. All six Lyapunov exponents of the driven system are plotted with the variation of ε for different values of Φ.

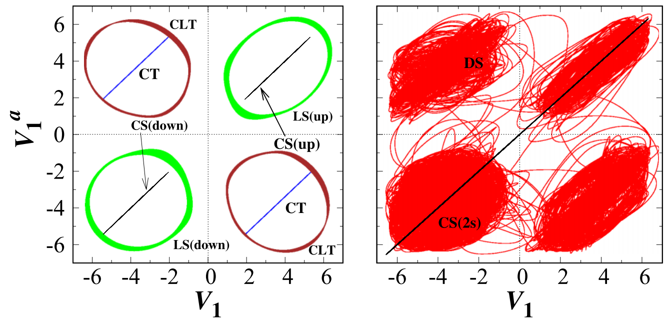

FIG. 14. V_1 of response vs V_1^a of auxiliary for the observed states, on the left CS(up), CS(down), LS(up), LS(down), CT, CLT, and on the right DS (red) and CS(2s) (Black). For LS and DS $\Phi = 0.2$ and $\epsilon = 1000$; for CT, CS(up), and CS(down) $\Phi = 1.0$ and for CS(2s) $\Phi = 1.5$ at $\epsilon = 1500$.

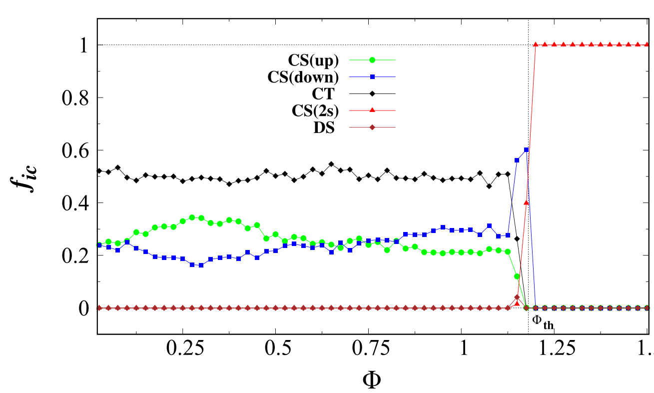

FIG. 15. Fraction of initial conditions, f_{ic} leading to different synchronized states as a function of timescale parameter Φ of the driving signal for fixed coupling ($\varepsilon = 1500$), considering 10^3 random initial conditions at each Φ.

TABLE II. Asymptotic growth rate, K at $c = 2$ and the median of K, K_m are shown for different values of Φ. The coupling parameter is fixed to $\varepsilon = 1000$.

Φ	K	K_m
0.2	−0.01149	0.01121
0.5	0.03480	0.18056
1.0	0.85941	0.97902
1.5	0.98545	0.99274

where variance and covariance are defined in the usual manner:

$$\mathrm{cov}(x_1, x_2) = \frac{1}{q}\sum_{j=1}^{q}[x_1(j) - \bar{x}_1][x_2(j) - \bar{x}_2],$$

with $\bar{x}_1 = \frac{1}{q}\sum_{j=1}^{q} x_1(j)$ and

$$\mathrm{var}(x_1) = \mathrm{cov}(x_1, x_1). \tag{17}$$

Furthermore, 100 random choices of c in the interval $(0,\pi)$ are taken and K is calculated for each c. The median of these K values is obtained as K_m. The obtained values of K at $c = 2$ and K_m for time series of V_1 at different Φ are tabulated in Table II. A K_m value close to zero indicates regular dynamics, whereas K_m close to one suggests chaotic dynamics. Therefore, the values of K_m suggest that as Φ increases from 0.2 to 1.5, the dynamics of Chua's circuit changes from regular to chaotic.

We also obtain p vs q plots for different Φ shown in Fig. 16. When the p-q phase space is bounded, the dynamics of the underlying trajectory is regular [36], which can either be periodic or quasiperiodic. Also, the modified mean squared displacement $D(n)$ is confined within a range for $\Phi = 0.2$ and 0.5, which shows that the nature of the oscillations of Chua's circuit at $\varepsilon = 1000$ (where $\lambda_m \approx 0$) is regular. On the other hand, the dynamics is chaotic when the p-q phase portrait is diffusive. $D(n)$ grows linearly with n, and the slope quantifies the nature of trajectories as chaotic for $\Phi = 1.0$ and $\Phi = 1.5$, in addition to K being close to 1. Clearly, at a fixed coupling ($\varepsilon = 1000$), the dynamics of Chua's circuit go from regular when the timescale of forcing is slow to chaotic when the timescales of the drive are comparable to the response system. To ascertain the regular behavior of Chua's circuit in the $\lambda_m \approx 0$ region, we further analyze the trajectories by using other measures such as FFT and recurrence plots of the time-series data.

B. FFT

We do the fast Fourier transform (FFT) of the time series V_1 to know the dominant frequencies. In Fig. 17, the FFT plots of the time series show a clear single peak for $\Phi = 0.2$ and 0.5, indicating the periodic nature of the time series. As Φ increases, other harmonics emerge and there is a spread in the FFT plot. The amplitude of these harmonics increases with an increase in Φ, and the dynamics becomes chaotic for higher values of Φ [Figs. 17(c) and 17(d)].

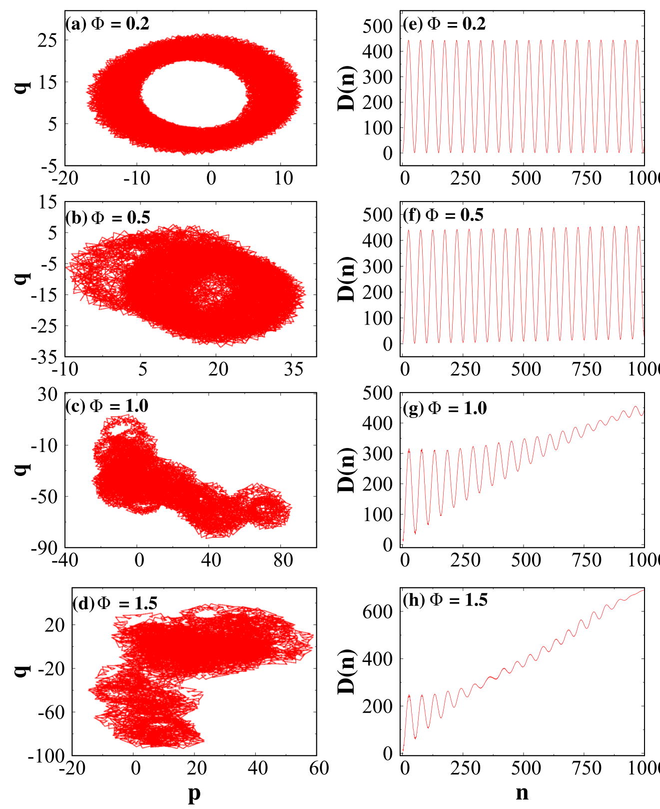

FIG. 16. The p-q phase portraits are shown in the left panels (a)–(d) with their respective modified mean square displacement $D(n)$ in the right panels (e)–(h) for different values of Φ at fixed coupling $\varepsilon = 1000$. The system is simulated for 10^6 time steps with the sampling interval $T = 100$ and $N = 10^4$. The plots are shown for $c = 2$.

C. Recurrence plots

Recurrence plots (RPs) [37] are used to study the recurrences of the phase-space trajectories. Consider a dynamical system in d-dimensional phase space represented by the

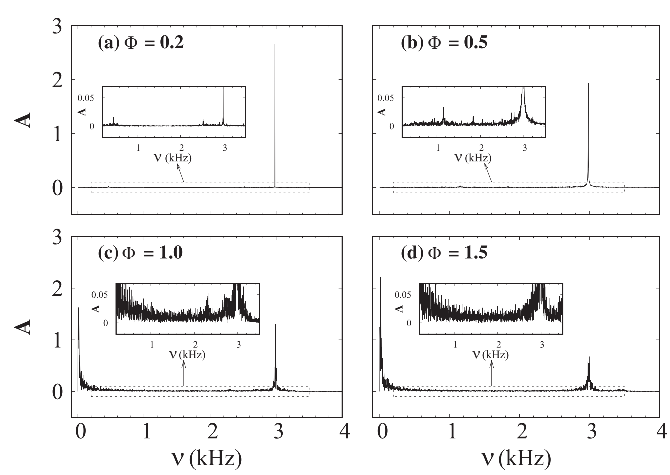

FIG. 17. FFT of the time series V_1 for different values of the Φ at $\varepsilon = 1000$. The y axis represents the amplitude, A of the frequency components, while the x axis denotes the frequency ν. The inset shows a magnified image of the amplitudes in the marked (box with dotted lines) frequency range.

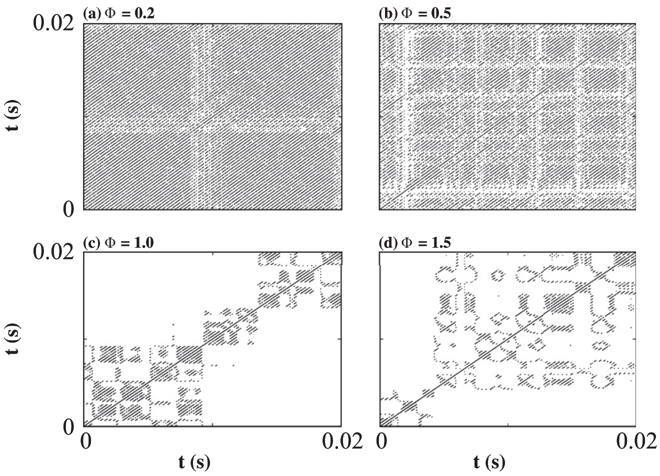

FIG. 18. RPs computed from the time-series of response Chua's circuit for different values of Φ. The value of $\delta = 0.05$.

trajectory $\{\boldsymbol{x}_i\}$ for $i = 1, \dots, N$. The binary recurrence matrix is defined as

$$R_{ij} = \Theta(\delta - \|\boldsymbol{x}_i - \boldsymbol{x}_j\|), \quad i, j = 1, \dots, N, \tag{18}$$

where Θ is the Heaviside function and $\|.\|$ is the norm of the distance between two points. δ defines the threshold of the norm below which the pairs of phase space points are considered to recur.

For our case, we construct the RPs from the time series of all three variables of the driven Chua's circuit for different values of Φ, fixing $\varepsilon = 1000$. The plots are shown in Fig. 18. For slow drive ($\Phi = 0.2$), we observe parallel equispaced lines in most regions of RPs [see Figs. 18(a) and 18(b)], which suggest the periodic nature of the driven Chua oscillator with intermittent bursts of irregular behavior when the system is evolved for a long time. As the timescale of the driving signal increases and approaches the timescale of the response, we notice that the irregular behavior becomes more frequent and the trajectory becomes chaotic [37,38]. These RPs show signatures of intermittency route to chaos [39] in Chua's circuit dynamics as Φ increases. To investigate the type of intermittency in the response system in the coupling region where $\lambda_m = 0$, we look at the behavior for the periodic or laminar phase of the trajectory at different Φ as shown in Fig. 19. For high frequency of the drive ($\Phi = 1.0$, 1.5), we observe the laminar phase has black squares with perforated edges which suggest type-II intermittency [40], while for low frequency of the drive ($\Phi = 0.2$, 0.5) the periodic nature of the driven system can be seen.

From the analysis of time-series of the response variables at a fixed coupling strength, we can conclude that a slow drive induces periodicity in the dynamics of the response system reflected in the value of the largest CLE close to zero. As the timescale of the drive increases and becomes comparable to that of the response, the response dynamics becomes irregular and chaotic. However, we would like to point out that our analysis does not exclude the possibility of quasiperiodicity in the dynamics of the response system which needs to be investigated in more detail.

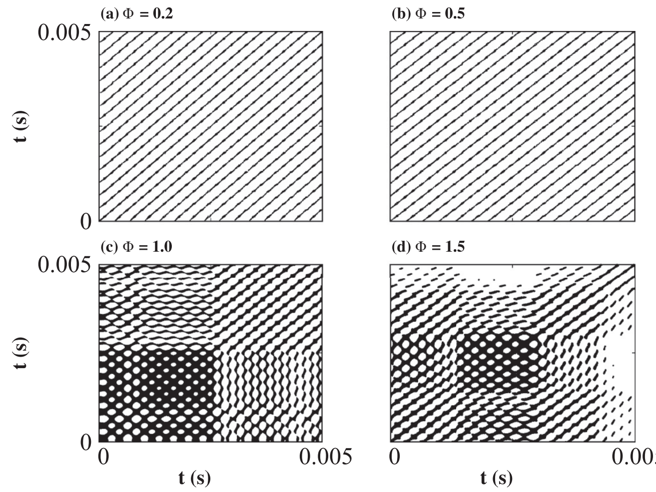

FIG. 19. The RPs of the laminar phase of the trajectory of a driven Chua circuit obtained for different values of Φ is shown. The δ value is taken to be 0.5, which is 10% of the diameter of the single scroll attractor.

VI. SUMMARY

In this work, we study the effect of a variable timescale of the drive on the response of Chua's circuit in the chaotic regime. The driving signal is chaotic and drawn from a common base Colpitts oscillator. We observe that when the timescale of the drive is much slower than the response, and the driving strength is above a certain threshold, Chua's oscillator exhibits bistability with coexisting chaotic attractors. These multistable attractors are different from the double-scroll chaotic attractor of the uncoupled Chua's circuit in the sense that they are single-scroll and occupy a much smaller region in phase space. When an auxiliary system is considered to explore the prospects of generalized synchronization in such systems, we observe that the drive and auxiliary units show remote synchronization where the two units have equal average frequency yet their dynamical variables are correlated to each other in different ways. In addition to the scenario when the response and auxiliary systems are in complete synchrony (RS-I), there could be lag synchronization (RS-III) or correlated trajectories (RS-II and RS-IV) of the two Chua circuits, indicating new forms of remote synchrony between the uncoupled response and auxiliary units. The existence of complete synchrony between response and auxiliary units implies generalized synchrony in these drive-response systems. The parameter region where RS-III and RS-IV coexist is characterized by the largest conditional Lyapunov exponent close to zero. We analyzed this region using various tools such as the 0–1 chaos test, a FFT, and recurrence plots and found that the dynamics of Chua's circuit is periodic in the region of slow forcing and becomes chaotic through intermittency as the timescale of the drive increases and becomes equivalent to that of the response. The region where lag synchronization and correlated trajectories occur diminishes as the frequency of the drive approaches the frequency of the response. Therefore, such kinds of states and hence RS are not possible if the drive and response variables evolve at similar timescales. We have also checked the case when the frequency of the drive is higher than the inherent frequency of the response and observed that, in this setup, the dynamics of the response is dependent on the nature of the drive; for example, a symmetric drive can give bistability with two coexisting single-scroll attractors whereas an asymmetric drive can favor one type of attractor over the other. Although the results presented in this paper are for the dimensional model, the results have been found consistent with those obtained from the equivalent nondimensional model.

The multistability induced in the present system is the result of timescale mismatch between drive and response, and hence the mechanism leading to this multistability seems to be different from the multistability induced by coupling reported earlier [41], where the coupling modifies the effective parameter to the values where the response system is inherently multistable. To check the generality of our results, we checked our results for different types of driving signals, for instance, Chua's circuit driven by Rössler oscillator and observed qualitatively similar states. It will be interesting to investigate the dynamics of Chua's circuit driven by periodic and quasiperiodic signals with variable frequency, which is part of our ongoing research [42]. Our preliminary investigation suggests that, in addition to the multistability observed in the case of chaotic drive, we can observe other kinds of multistable behavior involving resonance response of Chua's circuit. We believe that our results open up several interesting directions to explore; for instance, the implications of reported multistable RS states in networks with hub structures. In a recent work by Gomes *et al.* [43], chaotic hysteresis is reported in Chua's circuit driven by slow voltage forcing. Hysteresis is often observed in systems that have multistability; therefore, another possible direction to explore could be to look for the possibility of chaotic hysteresis in coupled systems with mismatched timescales.

ACKNOWLEDGMENTS

T.M. and A.S. acknowledge the resources provided by PARAM Shivay computational facility at the Indian Institute of Technology, Varanasi. S.R.U. is thankful to Banaras Hindu University for financial support under the Institute of Eminence (IoE) scheme. We thank Awadhesh Prasad for useful discussions.

DATA AVAILABILITY

There are no publicly available research data or software supporting this paper. Requests for further information or data should be sent to the authors.

[1] A. Pikovsky, M. Rosenblum, and J. Kurths, *Synchronization: A Universal Concept in Nonlinear Sciences* (Cambridge University Press, Cambridge, 2001).
[2] E. Ott, *Chaos in Dynamical Systems* (Cambridge University Press, Cambridge, 1993).
[3] S. Boccaletti, J. Kurths, G. Osipov, D. L. Valladares, and C. S. Zhou, The synchronization of chaotic systems, Phys. Rep. **366**, 1 (2002).
[4] S. Bowong, Stability analysis for the synchronization of chaotic systems with different order: Application to secure communications, Phys. Lett. A **326**, 102 (2004).
[5] E. Padmanaban, R. Banerjee, and S. K. Dana, Targeting and control of synchronization in chaotic oscillators, Int. J. Bifurcation Chaos Appl. Sci. Eng. **22**, 1250177 (2012).
[6] L. Kocarev and U. Parlitz, General approach for chaotic synchronization with applications to communication, Phys. Rev. Lett. **74**, 5028 (1995).
[7] W. Kinzel, A. Englert, and I. Kanter, On chaos synchronization and secure communication, Philos. Trans. R. Soc. A **368**, 379 (2010).
[8] V. S. Afraimovich, N. N. Verichev, and M. I. Rabinovich, Stochastic synchronization of oscillations in dissipative systems, Radiophys. Quantum Electron. **29**, 795 (1986).
[9] L. M. Pecora and T. L. Carroll, Synchronization in chaotic systems, Phys. Rev. Lett. **64**, 821 (1990).
[10] K. Murali and M. Lakshmanan, Drive-response scenario of chaos synchronization in identical nonlinear systems, Phys. Rev. E **49**, 4882 (1994).
[11] N. F. Rulkov and M. M. Sushchik, Experimental observation of synchronized chaos with frequency ratio 1:2, Phys. Lett. A **214**, 145 (1996).
[12] A. Kittel, J. Parisi, and K. Pyragas, Generalized synchronization of chaos in electronic circuit experiments, Phys. D **112**, 459 (1998).
[13] N. F. Rulkov, M. M. Sushchik, L. S. Tsimring, and H. D. I. Abarbanel, Generalized synchronization of chaos in directionally coupled chaotic systems, Phys. Rev. E **51**, 980 (1995).
[14] H. D. I. Abarbanel, N. F. Rulkov, and M. M. Sushchik, Generalized synchronization of chaos: The auxiliary system approach, Phys. Rev. E **53**, 4528 (1996).
[15] A. Bergner, M. Frasca, G. Sciuto, A. Buscarino, E. J. Ngamga, L. Fortuna, and J. Kurths, Remote synchronization in star networks, Phys. Rev. E **85**, 026208 (2012).
[16] L. O. Chua, The genesis of Chua's circuit, Archiv für Elektronik und Übertragungstechnik **46**, 250 (1992).
[17] L. O. Chua, Chua's circuit: An overview ten years later, J. Circuits, Syst. Comput. **04**, 117 (1994).
[18] G.-Q. Zhong and F. Ayrom, Experimental confirmation of chaos from Chua's circuit, Int. J. Circuit Theory Appl. **13**, 93 (1985).
[19] K. Murali, M. Lakshmanan, and L. O. Chua, The simplest dissipative nonautonomous chaotic circuit, IEEE Trans. Circuits Syst. I **41**, 462 (1994).
[20] L. O. Chua, L. Kocarev, K. Eckert, and M. Itoh, Experimental chaos synchronization in Chua's circuit, Int. J. Bifurcation Chaos Appl. Sci. Eng. **02**, 705 (1992).
[21] Z. Liu, J. Ma, G. Zhang, and Y. Zhang, Synchronization control between two Chua's circuits via capacitive coupling, J. Comp. App. Math. **360**, 138 (2019).
[22] K. Murali and M. Lakshmanan, Effect of sinusoidal excitation on the Chua's circuit, IEEE Trans. Circuits Syst. I **39**, 264 (1992).

[23] M. Itoh, H. Murakami, and L. O. Chua, Experimental study of forced Chua's oscillator, Int. J. Bifurcation Chaos **04**, 1715 (1994).

[24] P. K. Roy and A. Basuray, A high frequency chaotic signal generator: A demonstration experiment, Am. J. Phys. **71**, 34 (2003).

[25] J. M. Cruz and L. O. Chua, An IC chip of Chua's circuit, IEEE Trans. Circuits Syst. II **40**, 614 (1993).

[26] E. Tlelo-Cuautle and J. M. Muñoz-Pacheco, Numerical simulation of Chua's circuit oriented to circuit synthesis, Int. J. Nonlinear Sci. Numer. Simul. **8**, 249 (2007).

[27] E. Lv, Chua's circuit simulation experiment based on saturation function, J. Phys.: Conf. Ser. **2078**, 012026 (2021).

[28] The initial condition for Chua's oscillator is taken to be $(V_1, V_2, I_L) = (0.5, 0.3, -0.001)$.

[29] For the simulations, the initial conditions for Chua's and Colpitts oscillators are taken randomly in the range -1.0 to 1.0 for V_1 and V_2 (in units of volts) and -0.005 to 0.005 for I_L (in units of Amperes).

[30] M. P. Kennedy, Chaos in the Colpitts oscillator, IEEE Trans. Circuits Syst. I **41**, 771 (1994).

[31] T. Matsumoto, L. O. Chua, and M. Komuro, The double scroll, IEEE Trans. Circuits Syst. **32**, 797 (1985).

[32] M. G. Rosenblum, A. S. Pikovsky, and J. Kurths, From phase to lag synchronization in coupled chaotic oscillators, Phys. Rev. Lett. **78**, 4193 (1997).

[33] Y. Kuramoto and D. Battogtokh, Coexistence of coherence and incoherence in nonlocally coupled phase oscillators, Nonlinear Phenom. Complex Syst. **5**, 380 (2002).

[34] D. M. Abrams and S. H. Strogatz, Chimera states for coupled oscillators, Phys. Rev. Lett. **93**, 174102 (2004).

[35] G. A. Gottwald and I. Melbourne, On the implementation of the 0–1 test for chaos, J. Appl. Dyn. Syst. **8**, 129 (2009).

[36] R. Gopal, A. Venkatesan, and M. Lakshmanan, Applicability of 0-1 test for strange nonchaotic attractors, Chaos **23**, 023123 (2013).

[37] J.-P. Eckmann, S. O. Kamphorst, and R. Ruelle, Recurrence plots of dynamical systems, Europhys. Lett. **4**, 973 (1987).

[38] L. Kabiraj and R. I. Sujith, Nonlinear self-excited thermoacoustic oscillations: Intermittency and flame blowout, J. Fluid Mech. **713**, 376 (2012).

[39] Y. Pomeau and P. Manneville, Intermittent transition to turbulence in dissipative dynamical systems, Commun. Math. Phys. **74**, 189 (1980).

[40] K. Klimaszewska and J. J. Zebrowski, Detection of the type of intermittency using characteristic patterns in recurrence plots, Phys. Rev. E **80**, 026214 (2009).

[41] S. R. Ujjwal, N. Punetha, R. Ramaswamy, M. Agrawal, and A. Prasad, Driving-induced multistability in coupled chaotic oscillators: Symmetries and riddled basins, Chaos **26**, 063111 (2016).

[42] T. Mahanty, A. Saxena, and S. R. Ujjwal (unpublished).

[43] I. Gomes, W. Korneta, S. G. Stavrinides, R. Picos, and L. O. Chua, Experimental observation of chaotic hysteresis in Chua's circuit driven by slow voltage forcing, Chaos Solit. Fractals **166**, 112927 (2023).